NeuroImage: Clinical 34 (2022) 102987

Contents lists available at ScienceDirect

NeuroImage: Clinical

journal homepage: www.elsevier.com/locate/ynicl

Brain microstructural antecedents of visual difficulties in infants born very preterm

Rahul Chandwani [a], Karen Harpster [a,b,c], Julia E. Kline [a], Ved Mehta [a], Hui Wang [e,f], Stephanie L. Merhar [a,d], Terry L. Schwartz [g,h], Nehal A. Parikh [a,d,*]

[a] Center for Prevention of Neurodevelopmental Disorders, Perinatal Institute, Cincinnati Children's Hospital Medical Center, Cincinnati, OH, United States
[b] Division of Occupational Therapy and Physical Therapy, Cincinnati Children's Hospital Medical Center, Cincinnati, OH, United States
[c] Department of Rehabilitation, Exercise, and Nutrition Sciences, College of Allied Health Sciences, University of Cincinnati, Cincinnati, OH, United States
[d] Department of Pediatrics, University of Cincinnati College of Medicine, Cincinnati, OH, United States
[e] Imaging Research Center, Cincinnati Children's Hospital Medical Center, Cincinnati, OH, United States
[f] MR Clinical Science, Philips, Cincinnati, OH, United States
[g] Division of Pediatric Ophthalmology, Cincinnati Children's Hospital Medical Center, Cincinnati, OH, United States
[h] Department of Ophthalmology, University of Cincinnati College of Medicine, Cincinnati, OH, United States

ARTICLE INFO

Keywords:
Very preterm
Cerebral visual impairment
Diffusion MRI
White matter
Neonatology

ABSTRACT

Infants born very preterm (VPT) are at risk of later visual problems. Although neonatal screening can identify ophthalmologic abnormalities, subtle perinatal brain injury and/or delayed brain maturation may be significant contributors to complex visual-behavioral problems. Our aim was to assess the micro and macrostructural antecedents of early visual-behavioral difficulties in VPT infants by using diffusion MRI (dMRI) at term-equivalent age.

We prospectively recruited a cohort of 262 VPT infants (≤32 weeks gestational age [GA]) from five neonatal intensive care units. We obtained structural and diffusion MRI at term-equivalent age and administered the Preverbal Visual Assessment (PreViAs) questionnaire to parents at 3–4 months corrected age. We used constrained spherical deconvolution to reconstruct nine white matter tracts of the visual pathways with high reliability and performed fixel-based analysis to derive fiber density (FD), fiber-bundle cross-section (FC), and combined fiber density and cross-section (FDC). In multiple logistic regression analyses, we related these tract metrics to visual-behavioral function.

Of 262 infants, 191 had both high-quality dMRI and completed PreViAs, constituting the final cohort: mean (SD) GA was 29.3 (2.4) weeks, 90 (47.1%) were males, and postmenstrual age (PMA) at MRI was 42.8 (1.3) weeks. FD and FC of several tracts were altered in infants with (N = 59) versus those without retinopathy of prematurity (N = 132). FDC of the left posterior thalamic radiations (PTR), left inferior longitudinal fasciculus (ILF), right superior longitudinal fasciculus (SLF), and left inferior fronto-occipital fasciculus (IFOF) were significantly associated with visual attention scores, prior to adjusting for confounders. After adjustment for PMA at MRI, GA, severe retinopathy of prematurity, and total brain volume, FDC of the left PTR, left ILF, and left IFOF remained significantly associated with visual attention.

Early visual-behavioral difficulties in VPT infants are preceded by micro and macrostructural abnormalities in several major visual pathways at term-equivalent age.

Abbreviations: CVI, Cerebral Visual Impairment; CSD, Constrained Spherical Deconvolution; CC, Corpus Callosum; FC, Fiber-Bundle Cross-Section; FD, Fiber Density; FDC, Fiber Density and Cross-Section; fOD, Fiber Orientation Distribution; IFOF, Inferior Fronto-Occipital Fasciculus; ILF, Inferior Longitudinal Fasciculus; GA, Gestational Age; PTR, Posterior Thalamic Radiations; PMA, Postmenstrual Age; ROP, Retinopathy of Prematurity; SLF, Superior Longitudinal Fasciculus; TEA, Term-Equivalent Age; VPT, Very Preterm.

* Corresponding author at: Cincinnati Children's Hospital Medical Center, 3333 Burnet Avenue, MLC 7009, Cincinnati, OH 45229, United States.
E-mail address: nehal.parikh@cchmc.org (N.A. Parikh).

https://doi.org/10.1016/j.nicl.2022.102987
Received 2 November 2021; Received in revised form 12 February 2022; Accepted 7 March 2022
Available online 9 March 2022

1. Introduction

Annually, 15 million infants worldwide are born preterm (Walani, 2020). Despite advances in neonatal care, infants born very preterm (VPT, ≤ 32 weeks gestational age [GA]) are at high risk of mortality or adverse neurodevelopmental outcomes (Pascal et al., 2018). An estimated 20,000 VPT infants globally develop blindness or severe visual impairment from retinopathy of prematurity (ROP), and a further 12,300 have mild to moderate visual impairment (Blencowe et al., 2013). In addition to ophthalmologic deficits (e.g., low visual acuity, refractive errors, strabismus), VPT infants can have brain injury that affects post-retinal processing of visual information (Cioni et al., 1997; O'Connor et al., 2007; Leung et al., 2018). Damage to the visual cortical pathways results in cerebral visual impairment (CVI), a condition of higher-order visual dysfunction, which includes difficulties in visual perception, visual-motor integration, and object recognition (Philip and Dutton, 2014). CVI encompasses a broad range of comorbid disorders, as complex visual-behavioral abnormalities may present with ophthalmologic/oculomotor symptoms, intellectual disability, and cerebral palsy (Fazzi et al., 2007; Jakobson and Taylor, 2009). This variation poses a challenge for the clinical diagnosis and treatment of CVI. Cerebral visual deficits that escape detection and persist into adolescence greatly impact a child's learning, cognition, and behavior (Leung et al., 2018). A better understanding of the clinical and cerebral antecedents of such abnormalities is needed. Accurate tools are also needed to diagnose visual-behavioral problems early and promptly facilitate interventions.

Current ophthalmologic care and childhood vision screening programs focus on evaluating ocular structures, visual acuity, and refraction (American Academy of Pediatrics, 2003; Cotter et al., 2015). However, these methods are insufficient for assessing the integration of visual information with cerebral functions (Pueyo et al., 2014). Advanced neuroimaging techniques at term-equivalent age (TEA) show promise in identifying sensitive and objective measures of neurodevelopmental impairments (Parikh, 2016). The visual system has been studied with these imaging modalities, and correlations exist between visual dysfunction in preterm infants and findings on MRI (Cioni et al., 2000; Guzzetta et al., 2001; Ricci et al., 2006; Shah et al., 2006). Diffusion MRI (dMRI) is a tool that provides insight into the microstructural development of the brain, and diffusion tensor imaging (DTI) metrics (i.e., fractional anisotropy, FA) are commonly used to examine white matter structural connectivity (Tournier et al., 2011). Several studies have used DTI to investigate the visual system in preterm infants, finding that decreased FA of the optic radiations was associated with worse visual function scores (Bassi et al., 2008; Berman et al., 2009; Thompson et al., 2013; Groppo et al., 2014). While these results implicate a role for the optic radiations in visual development, other white matter tracts of the visual network have not been extensively researched. Cerebral biomarkers of these tracts at TEA could improve our understanding of aberrant visual development in preterm populations and potentially contribute to early diagnosis.

The accuracy of the DTI model is limited in brain regions with crossing fibers (i.e., two or more differently oriented fiber bundles contributing to a single measured signal), present in approximately 90% of white matter voxels (Jeurissen et al., 2013). Crossing fibers introduce error into DTI-based tractography via false positive and false negative connections, and make it challenging to interpret metrics such as FA (Alexander et al., 2001; Tournier et al., 2011). To overcome the crossing fiber problem and better represent white matter microstructure, several advanced dMRI models have been developed, one of which is constrained spherical deconvolution, or CSD (Tournier et al., 2004). CSD requires high angular resolution diffusion imaging (HARDI) data with higher b-values (≥2000 s/mm^2) and models the diffusion signal in each voxel as a function of all fiber orientations present within the voxel, i.e., the fiber orientation distribution (fOD), which can be used to perform tractography (Tournier et al., 2004, 2007; Reijmer et al., 2012; Jeurissen et al., 2014; Auriat et al., 2015).

The fOD can also be used to derive quantitative measures of microscopic and macroscopic white matter morphology that are associated with 'fixels,' or fibers of a single orientation within a voxel (Raffelt et al., 2012, 2017). Thus, fixel-based analysis is advantageous over traditional voxel-based analysis for assessing changes in white matter, especially in regions with many crossing fibers (Dhollander et al., 2021). Fixel-based analysis calculates fiber density (FD), fiber-bundle cross-section (FC), and their combined metric, fiber density and cross-section (FDC), as relative measures of axonal morphology (Raffelt et al., 2017). Using histology, HARDI model estimates of fODs have been validated, with several studies also finding correlations between fixel-based metrics and white matter pathology (Leergaard et al., 2010; Malhotra et al., 2019; Rojas-Vite et al., 2019). We previously investigated sensorimotor white matter tracts in our VPT cohort and found strong independent associations of tract FD, FC, and FDC with early diagnosis of cerebral palsy (Chandwani et al., 2021). Our results suggested the potential of CSD and fixel-based analysis in identifying biomarkers of other neurodevelopmental impairments. To our knowledge, no prior study has used CSD-derived, fixel-based metrics to determine the antecedents of abnormal visual development in preterm infants.

In the current work, our goal is to investigate the micro and macrostructure of major visual pathways at TEA that may contribute to complex visual-behavioral problems in at-risk infants. By using a large cohort of VPT infants, advanced dMRI modeling techniques, and systematic tractography methods to query multiple white matter tracts, this study extends prior research and improves our understanding of the pathophysiology of CVI. To achieve this goal, we measured the macro and microstructure of the visual pathways, derived from dMRI at TEA, and determined their relationship with early visual difficulties in VPT infants. We used CSD to obtain fODs, perform tractography, and parse nine white matter tracts implicated in visual development. For each tract, we computed fixel-based metrics of white matter morphology. Our hypothesis was that visual tract FD, FC, and FDC at TEA would be positively associated with visual-behavioral assessment scores at 3–4 months corrected age.

2. Materials and methods

2.1. Study design

Between June 2017 and October 2019, we prospectively enrolled a multicenter cohort of 262 VPT infants born at or before 32 weeks GA from five regional, level-III neonatal intensive care units (NICUs). These NICUs included: (1) Cincinnati Children's Hospital Medical Center, (2) University of Cincinnati Medical Center, (3) Good Samaritan Hospital, (4) St. Elizabeth Healthcare, and (5) Kettering Medical Center. Infants were excluded if they had cyanotic heart disease or congenital/chromosomal anomalies of their central nervous system. This study was approved by the Cincinnati Children's Hospital Institutional Review Board. Written informed consent was provided by a parent or guardian of each infant, prior to enrollment and participation in the study.

2.2. Data acquisition

We acquired MRI data at Cincinnati Children's Hospital using a 3T Philips Ingenia MRI scanner (Best, the Netherlands) with a 32-channel head coil, as previously described (Chandwani et al., 2021). Subjects were imaged in natural sleep without sedation, between 39- and 44-weeks postmenstrual age (PMA). Before MRI scanning, each infant was fed and swaddled to promote natural sleep, as well as fitted with silicone earplugs for noise protection.

The dMRI protocol consisted of a 68-direction acquisition (phase encoding posterior to anterior) obtained in the axial plane with full brain coverage: 61 directions with b-values of 2000 s/mm^2 and 7 with b-values of 0 s/mm^2 (the b0s were distributed uniformly for intra-scan motion correction). In a separate acquisition, 6 more b0s were

obtained (phase encoding anterior to posterior). Scan parameters used in both acquisitions: echo time (TE) 88 ms, repetition time (TR) 5073 ms, flip angle = 90°, FOV 160x160 mm^2, 80 × 78 matrix size, 2 mm slices; multiband factor = 2; SENSE factor = 2, and scan time 6:27 min. The following acquisition parameters were used for the axial T2-weighted image: TE 166 ms, TR 18567 ms, flip angle = 90°, voxel dimensions 1.0x1.0x1.0 mm^3, and scan time 3:43 min.

2.3. Preverbal visual assessment (PreViAs)

The Preverbal Visual Assessment (PreViAs) questionnaire was administered to parents at 3–4 months corrected age, by a single masked assessor unaware of clinical and MRI data. PreViAs is a validated behavioral assessment of visual-integrative abilities, indicated for infants under 24 months of age. The assessment consists of 30 "yes or no" questions categorized into one or more of four domains of visual-behavioral function: visual attention, visual communication, visual motor coordination, and visual processing. The questions are summed (1 point per item) to obtain the four domain scores (Pueyo et al., 2014).

The identification of visual-behavioral difficulties remains challenging due to their varying clinical presentation. While inventories exist that assess visual-behavioral skills based on a structured clinical history-taking approach, these methods are not scored and do not provide normative outcomes. PreViAs domains exhibit high internal consistency, high test–retest reliability, and have been validated in infant populations with a comprehensive ophthalmologic test battery (Garcia-Ormaechea et al., 2014; Pueyo et al., 2014). A recent study by Lee et al. (2021) showed preterm infants had significantly lower scores in each PreViAs domain compared to term-born infants, and very preterm/very-low birth weight infants had significantly lower scores than moderate-late preterm infants.

We dichotomized PreViAs scores based on guidelines suggested by the developers of the questionnaire. These guidelines placed infants in a high-risk group based on a score cutoff (Garcia-Ormaechea et al., 2014; Pueyo et al., 2014). Abnormal domain scores were assigned using the following cutoffs, below which infants should be monitored for visual problems: visual attention score of $\leq$5 (max score = 11), visual communication score $\leq$2 (max score = 5), visual motor-coordination score $\leq$3 (max score = 13), and visual processing score $\leq$3 (max score = 20).

2.4. MRI preprocessing

Preprocessing of b2000 diffusion-weighted data was performed in MRtrix3 (https://www.mrtrix3.org), as previously described (Chandwani et al., 2021). Briefly, preprocessing steps included denoising and correcting Gibbs-ringing artifacts, motion artifacts, eddy current distortions, susceptibility-induced off-resonance field, and low-frequency intensity inhomogeneities. Using the median b0 white matter value, global intensity normalization was performed across subjects (Tournier et al., 2019; Chandwani et al., 2021).

2.5. CSD and Fixel-based analysis

HARDI data can be represented as the spherical convolution of a fiber response function (i.e., the expected signal from a single fiber population) and the fOD. By using an estimated response function as the deconvolution kernel, the fOD can be derived and then used for tractography (Tournier et al., 2007, 2019).

In MRtrix3, we used a single-tissue CSD pipeline to extract a white matter fOD from the dMRI signal measured in each voxel. First, we obtained an estimated response function for each subject by selecting the "Tournier" algorithm (Tournier et al., 2013). After preprocessing and intensity-normalization of b2000 data, we used the group-average response function as a deconvolution kernel to derive white matter fODs for all subjects (Chandwani et al., 2021).

Next, as described in Chandwani et al., we created a study specific fOD template from a subset of 40 subject fODs. No statistically significant differences were found in baseline variables between this subset of 40 subjects and the larger cohort.

To perform fixel-based analysis in MRtrix3 (Raffelt et al., 2017), the fOD template was segmented to generate a fixel template, shown in Fig. 1A-C. All subject fODs were warped and registered to the fOD template, and then also segmented to obtain fixels. Subject fixels were reoriented and assigned to template fixels, which was required for a 1-to-1 correspondence.

We performed probabilistic whole-brain tractography from the fOD template, and segmented nine white matter tracts of interest: the splenium of the corpus callosum (CC) and bilateral representations of the inferior longitudinal fasciculus (ILF), inferior fronto-occipital fasciculus (IFOF), superior longitudinal fasciculus (SLF), and posterior thalamic radiations (PTR). Lastly, we created tract masks in template space and computed the mean FD, FC, and FDC for fixels present within each mask (Raffelt et al., 2017; Tournier et al., 2019). These metrics represent the microscopic and macroscopic fiber morphology of our segmented white matter tracts. For more details, our group has published data on fixel-based metrics generated using this CSD methodology (Chandwani et al., 2021).

2.6. Tract segmentation

We used a multiple region-of-interest (ROI) approach in MRtrix3′s ROI Editor to segment nine white matter tracts from the whole-brain tractograph (Fig. 1D-F) that are associated with the visual pathways. For each tract, we created seed point, waypoint, and exclusion masks, which initiated/restricted tracking to fibers passing through designated ROIs. All ROIs were manually delineated based on prior knowledge of neuroanatomical landmarks (Wakana et al., 2007; Thompson et al., 2011; Kaur et al., 2014; Parikh et al., 2019) and the white matter fiber trajectories displayed by the group fixel template (Fig. 1A-C).

We imported our masks in combination into MRtrix3′s *tckedit* command to generate the full segmented white matter tract. Notably, the size and placement of each ROI were optimized iteratively (Chandwani et al., 2021). For all tracts, voxels with partial volume fractions, intermediate fiber directions, or extraneous fiber projections were included/excluded appropriately, after iteratively examining the completed tract trajectory. ROI placement and segmentation were performed by a single trained individual (RC), supervised and verified by the senior author (NAP) who has more than 15 years of experience in quantitative dMRI neuroimaging.

Fig. 2 shows the final segmentations for each of our nine tracts. All tracts (except for the splenium of the CC) were segmented individually for each hemisphere (see SI Appendix for detailed protocol). To ensure the reliability and reproducibility of our method, segmentation of the nine tracts was repeated three additional times by the first author and intra-rater reliability measures were assessed. The first segmentation attempt of each tract was used to calculate fixel-based metrics for regression analyses. To assess the specificity of our results, we also segmented the bilateral uncinate fasciculus using our previously published methods (Chandwani et al., 2021).

2.7. Statistical analyses

Intra-class correlation coefficients (ICC) and Dice similarity index were used to assess the reliability and reproducibility of our tract segmentation protocol. To calculate ICC, fixel-based metrics were obtained for each tract in the initial two segmentation attempts. For Dice similarity index, we created an intersection mask of the two segmentations (based on their voxel-wise overlap), and then quantified the number of voxels present within each tract mask (Chandwani et al., 2021).

To identify potential confounders of visual development, we examined clinical factors of our cohort, such as maternal antenatal steroids

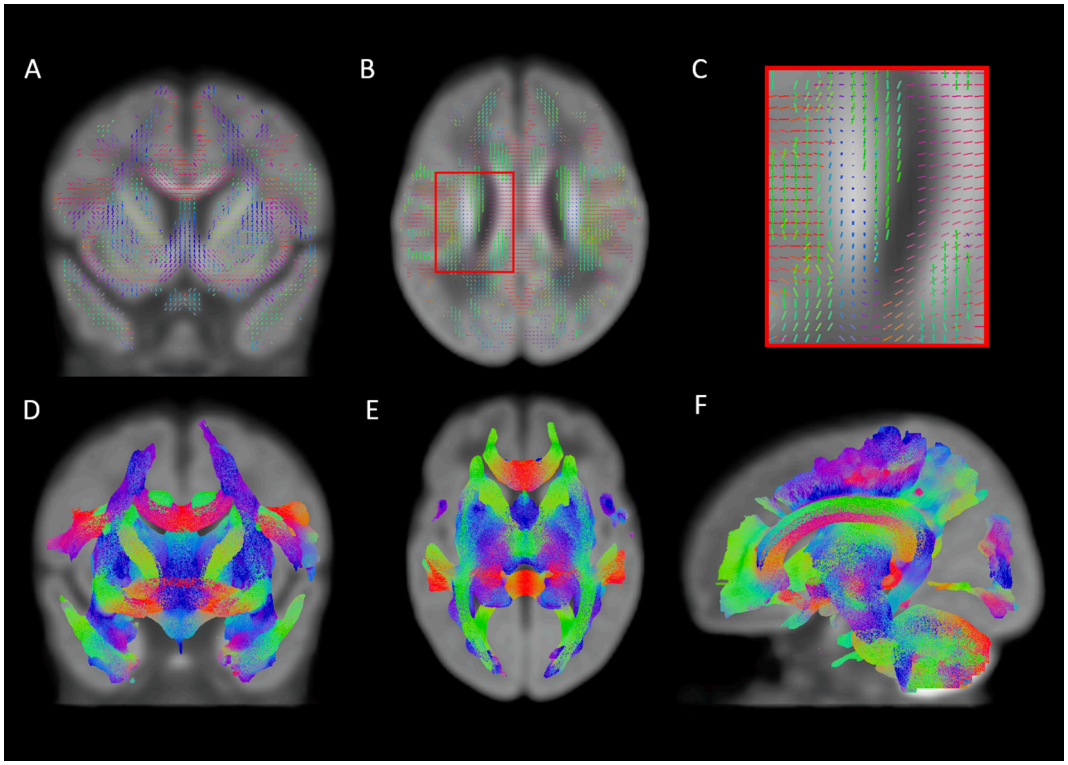

Fig. 1. Single tissue constrained spherical deconvolution (CSD) fixel template and whole brain tractograph displayed in MRtrix3. (A) Coronal view of the CSD fixel template demonstrating the fiber orientation distribution (fOD) for all brain voxels (B) Axial view of the same fixel template as in A with a region of interest placed in the right corona radiata. (C) Magnified view of the fOD voxels from the region of interest highlighted in B. (D-F) Whole-brain tractograph produced from the fOD template to segment and generate all white matter tracts in coronal, axial, and sagittal orientations, respectively. Color indicates fiber trajectory: green (anterior to posterior), red (left to right), and blue/purple (superior to inferior) fibers. (For interpretation of the references to color in this figure legend, the reader is referred to the web version of this article.)

and magnesium therapy, caffeine therapy, GA, PMA at MRI, sex, severe bronchopulmonary dysplasia (BPD), postnatal corticosteroids for BPD prevention/treatment, postnatal sepsis (culture-positive), and severe retinopathy of prematurity (ROP).

In the fixel-based framework, proposed by Raffelt et al. (2017), intracranial volume is used as a covariate for FC and FDC analyses. For our VPT cohort, total brain volume (derived using the developing Human Connectome Project pipeline (Makropoulos et al., 2018) as described in our prior study (Kline et al., 2020b)), was positively correlated with FC and FDC but not FD ($r = 0.5–0.6$ for FDC; 0.8–0.9 for FC; and 0.1–0.3 for FD). After correcting for PMA at MRI, volume remained significantly associated with FC and FDC. Therefore, we corrected our FC and FDC multivariable regression models with total brain volume in addition to the other identified clinical confounders. We used a Shapiro-Wilk Test to assess for normality, and a Mann Whitney Rank Sum Test or Chi Square Test to compare baseline variables: (1) between the excluded subjects and the final cohort used in the analysis, and (2) between the subset of 40 subjects used to create the fOD template and the total population.

To determine the relationship between fixel-based metrics for each tract and the four abnormalities identified on the PreViAs questionnaires, we used logistic regression analyses, with and without adjusting for significant confounders. In a separate analysis, we determined the relationship between fixel-based metrics and ROP diagnosis for infants in our cohort, as ROP is associated with abnormal/delayed brain maturation in preterm infants (Kline et al., 2019). Two-sided p-values of < 0.05 were considered statistically significant. We did not correct for multiple comparisons because of the preliminary nature of this study (Rothman, 1990). All statistical analyses were performed in STATA 13.1.

2.8. Data and code availability statement

Datasets and code used in this study are available upon request to the corresponding author.

3. Results

3.1. Demographics

Of the original 262 VPT infants with b2000 dMRI data, 33 were excluded in CSD processing or fixel-based analysis: 6 subjects had bright or dark artifacts that interfered with global intensity normalization; 23 had missing brain regions at the periphery of their diffusion-weighted scans (a 1-to-1 correspondence of subject fixels to template fixels is required for fixel-based analysis); 2 had suboptimal alignment with the fOD template, and 2 more had extreme ventriculomegaly causing poor registration of their fOD to the template. 191 (83%) of the remaining 229 infants had completed PreViAs scores at 3–4 months corrected age.

Demographic and clinical variables for infants included in the final cohort and infants excluded are shown in Table 1. Global brain abnormality score (as defined by Kidokoro et al., 2013) was used to assess structural injuries and delayed brain maturation for infants in our cohort (Median: 1, IQR: 4), as previously described (Harpster et al. 2021). 141 (73.8%) VPT infants had no injury on sMRI, 34 (17.8%) had mild injury, 8 (4.2%) had moderate injury, and 8 (4.2%) had severe injury.

Apart from global brain abnormality score, there were no significant differences in these variables between the 71 excluded infants [mean (SD) GA of 28.6 (2.6) weeks, PMA at MRI of 42.5 (1.3) weeks, birth weight of 1358 (477) grams, and 56% male] and the final cohort of 191 infants.

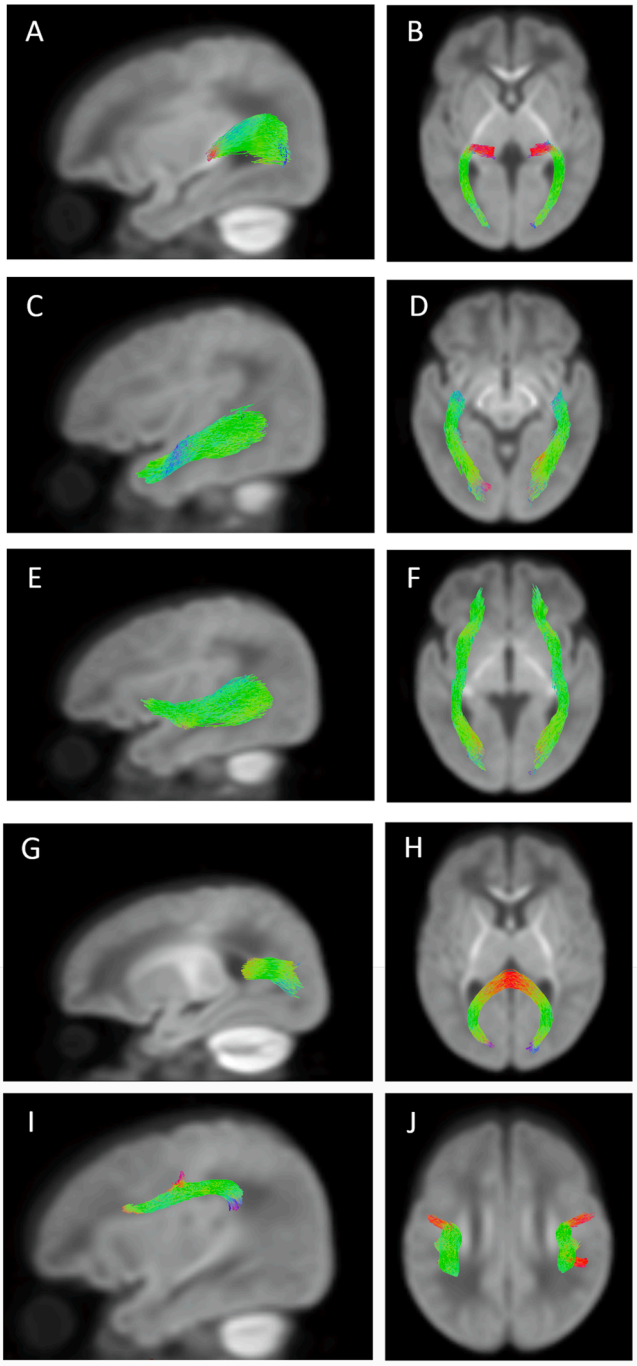

Fig. 2. Segmented White Matter Tracts of the Visual Pathways in Sagittal and Axial Orientations. A&B) posterior thalamic radiations; C&D) inferior longitudinal fasciculus; E&F) inferior fronto-occipital fasciculus; G&H) splenium of the corpus callosum; I&J) superior longitudinal fasciculus. Color indicates fiber trajectory: green (anterior to posterior), red (left to right), and blue/purple (superior to inferior) fibers. (For interpretation of the references to color in this figure legend, the reader is referred to the web version of this article.)

3.2. Reliability and reproducibility

The intra-rater reliability of tract segmentations, determined by ICC and Dice similarity index, is displayed in Supplementary Table S3. Across all tracts, the ICC for the FDC metric ranged from 0.998 to 0.999 and the Dice similarity index ranged from 0.922 to 0.986. High ICC and Dice similarity index suggest that our systematic, iterative tractography protocol is reliable and reproducible.

Table 1
Baseline characteristics of very preterm infants in the final cohort and infants excluded.

Clinical Variables*	VPT Infants in Final Cohort (N = 191)	VPT Infants Excluded (N = 71)	P-value
Maternal antenatal steroids, N (%)	178 (93.2%)	63 (88.7%)	0.237
Maternal magnesium therapy, N (%)	159 (83.2%)	58 (81.7%)	0.876
Gestational age at birth, weeks	29.3 (2.4)	28.6 (2.6)	0.243
Birth weight, grams	1273 (425)	1358 (477)	0.212
Male, N (%)	90 (47.1%)	40 (56.3%)	0.853
Head circumference at birth, cm	26.6 (3.1)	27.1 (3.1)	0.247
Postnatal corticosteroids, N (%)	18 (9.4%)	6 (8.5%)	0.808
Sepsis (culture positive), N (%)	20 (10.5%)	5 (7.0%)	0.280
Caffeine therapy, N (%)	139 (72.8%)	50 (70.4%)	0.706
Severe retinopathy of prematurity, N (%)	9 (4.7%)	4 (5.6%)	0.487
Severe bronchopulmonary dysplasia, N (%)	30 (15.7%)	13 (18.3%)	0.613
ROP, N (%)	59 (30.9%)	20 (28.2%)	0.670
BPD, N (%)	76 (39.8%)	29 (40.8%)	0.877
Postmenstrual age at MRI scan, weeks	42.8 (1.3)	42.5 (1.3)	0.074
Global brain abnormality score, median (IQR)	1 (4)	2 (4)	*0.017*

*All values are mean (SD) unless otherwise noted.

3.3. PreViAs domain analysis

As shown in Table 2, our final cohort had a median PreViAs visual attention score of 10 (IQR: 3; range: 3 to 11), median visual communication score of 4 (IQR: 2; range: 0 to 5), median visual motor coordination score of 6 (IQR: 3; range: 1 to 10), and median visual processing score of 5 (IQR: 3; range: 0 to 12). Using our pre-defined PreViAs domain cutoffs, we identified difficulties in the domains of visual attention, visual communication, visual motor coordination, and visual processing in 9 (4.7%), 19 (9.9%), 30 (15.7%), and 48 (25.1%) infants, respectively. In all, 55 (28.8%) of the 191 VPT infants exhibited signs of early difficulties in one or more of these four visual domains. These infants had a median global brain abnormality score of 2 (IQR: 4), compared to a median score of 1 (IQR: 3) for infants who did not demonstrate any difficulties across the four PreViAs domains.

3.4. Covariate selection

We completed between-group analyses for infants with and without abnormal PreViAs sub-scores (not shown). No consistent, significant differences were found between clinical variables when examined across all 4 PreViAs domains, including in sex, antenatal steroids, maternal magnesium therapy, or caffeine therapy. We included GA, PMA at MRI, and severe ROP in all multivariable logistic regression analyses, as they

Table 2
Descriptive statistics for PreViAs subdomains.

PreViAs Domain	Sample Size	Abnormal Scores N (%)	Mean (SD)	Median (IQR)	Range
Visual Attention	191	9 (4.7%)	9.27 (1.78)	10 (3)	3–11
Visual Communication	191	19 (9.9%)	3.80 (1.08)	4 (2)	0–5
Visual Motor Coordination	191	30 (15.7%)	5.27 (1.67)	6 (3)	1–10
Visual Processing	191	48 (25.1%)	4.93 (2.15)	5 (3)	0–12

*Abnormal scores determined after dichotomizing raw scores based on infant monitoring cutoffs.

are known to be associated with brain/visual development in prior studies and with visual tract morphology in our study, and therefore are known confounders. We also included total brain volume in multivariable logistic regression analyses of FC and FDC.

3.5. Macro and microstructural antecedents of PreViAs scores

Fig. 2 shows the final unilateral or bilateral segmentations for the ILF, IFOF, SLF, PTR, and splenium of the CC. Fixel-based metrics were calculated for each subject's tracts, and the mean (SD) values are shown in Supplementary Table 1. Table 3 displays the results of logistic regression analyses correlating FDC with PreViAs visual attention and visual communication domain scores, both with and without covariate correction.

In univariate analysis, FDC of the left PTR, left ILF, left IFOF, and right SLF were positively associated with visual attention scores. When confounders were included in the model, FDC of the left PTR, left ILF, and left IFOF remained significant. In univariate analysis, FDC of the left PTR, right ILF, left ILF, right IFOF, left IFOF, and right SLF were positively associated with visual communication scores, but none of these associations remained significant after adjusting for confounders. No significant associations were found between FDC of any visual pathway and visual motor coordination or visual processing domain score (Supplementary Table 2).

Secondary regression analyses with FD and FC for each PreViAs domain are shown in Tables 4-5. FD of the left PTR, left IFOF, and right SLF were positively associated with PreViAs visual attention scores, but only the right SLF remained significant in multivariable models. FC of the right PTR and right ILF and FD of the left IFOF were positively associated with PreViAs visual communication scores but did not remain significant following confounder adjustment. Supplementary Table S4 shows additional logistic regression analyses of PreViAs visual attention and visual communication scores with fixel-based metrics of the bilateral uncinate fasciculus.

3.6. Fixel-Based metrics and ROP

We also examined the relationship between fixel-based metrics and ROP diagnosis. Table 6 displays the mean (SD) FD, FC, and FDC values for VPT infants with and without ROP diagnosis. Significant differences were observed across these two groups in FD, FC, and FDC of the splenium, FC and FDC of the bilateral ILF, IFOF, FC of the bilateral SLF, PTR, and FDC of the left PTR.

4. Discussion

Our study is the first to assess the micro and macrostructure of major white matter visual pathways at TEA and determine their role in the pathophysiology of visual-behavioral difficulties in VPT infants. In a multi-center cohort, higher FD, FC, and FDC of the PTR, ILF, IFOF, and SLF were significantly associated with better early visual attention and visual communication abilities. This finding improves our understanding of the organization and structure of white matter fibers that potentially contribute to aberrant visual development in at-risk infants.

Brain pathology and/or abnormal brain development impact the diffusion-weighted signal of single fiber populations. In CSD, changes in diffusivity are detected as differences in the fOD, and thus, as differences in fixel-based metrics (Raffelt et al., 2012, 2017). FD, as proposed by Raffelt et al., is a microstructural measure of the intra-axonal volume of fibers, reflecting the local ability of white matter to relay information. For infants in our cohort, higher FD values indicate relatively larger intra-axonal volumes in the visual pathways at TEA, possibly due to a greater number of axons or increased axonal diameter per voxel (Raffelt et al., 2017). Since the number of voxels occupied by a fiber-bundle also impacts its ability to relay information, FC is a complementary measure of white matter morphology and accounts for differences in a bundle's intra-axonal volume occurring perpendicular to fiber orientation. Lower FC values for our infants could represent decreased myelination and/or white matter atrophy, resulting in thinner fiber bundles in the visual pathways at TEA (Raffelt et al., 2017). Because FD and FC are

Table 3
Logistic regression between tract fiber density and cross-section (FDC) and visual attention or visual communication score, with and without adjustment for known clinical confounders.

	Model corrected for PMA at MRI only		Model corrected for PMA at MRI and confounders*			Model corrected for PMA at MRI only		Model corrected for PMA at MRI and confounders*	
	Coef. (95% CI)	P Value	Coef. (95% CI)	P Value		Coef. (95% CI)	P Value	Coef. (95% CI)	P Value
Visual Attention[ξ]									
PTR(R)	6.390 (-5.451, 18.232)	0.290	6.206 (-10.101 22.513)	0.456	**PTR(L)**	11.956 (0.400, 23.513)	*0.043*	16.968 (0.347, 33.588)	*0.045*
ILF(R)	8.782 (-3.604, 21.168)	0.165	13.292 (-4.610, 31.194)	0.146	**ILF(L)**	11.581 (0.322, 22.840)	*0.044*	16.818 (0.980, 32.656)	*0.037*
IFOF(R)	9.245 (-3.162, 21.651)	0.144	10.189 (-7.455, 27.833)	0.258	**IFOF (L)**	13.349 (1.412, 25.286)	*0.028*	18.230 (1.453, 35.007)	*0.033*
SLF(R)	14.662 (0.189, 29.135)	*0.047*	12.861 (-4.395, 30.117)	0.144	**SLF(L)**	12.714 (-1.725, 27.153)	0.084	12.931 (-5.394, 31.255)	0.167
Splenium of CC	7.408 (-1.909, 16.726)	0.119	7.339 (-6.227, 20.905)	0.289					
Visual Communication[ξ]									
PTR(R)	8.678 (-0.093, 17.449)	0.052	7.943 (-3.575, 19.461)	0.177	**PTR(L)**	9.818 (1.228, 18.409)	*0.025*	8.699 (-2.750, 20.148)	0.136
ILF(R)	10.788 (1.742, 19.835)	*0.019*	11.941 (-0.223, 24.106)	0.054	**ILF(L)**	9.624 (1.330, 17.918)	*0.023*	9.058 (-1.814, 19.930)	0.102
IFOF(R)	9.472 (0.348, 18.596)	*0.042*	8.317 (-4.034, 20.667)	0.187	**IFOF (L)**	10.223 (1.454, 18.992)	*0.022*	9.263 (-2.557, 21.083)	0.125
SLF(R)	11.827 (1.526, 22.129)	*0.024*	9.278 (-2.358, 20.914)	0.118	**SLF(L)**	8.467 (-1.464, 18.397)	0.095	5.206 (-6.476, 16.888)	0.382
Splenium of CC	5.378 (-1.040, 11.797)	0.101	1.643 (-7.039, 10.324)	0.711					

*Adjusted for confounders including postmenstrual age at MRI scan, gestational age, severe retinopathy of the prematurity, and total brain volume.
Abbreviations: posterior thalamic radiations (PTR), inferior longitudinal fasciculus (ILF), inferior fronto-occipital fasciculus (IFOF), superior longitudinal fasciculus (SLF), corpus callosum (CC), postmenstrual age (PMA), right = R, left = L.
[ξ] PreViAs subdomain scores dichotomized based on monitoring cutoffs.

Table 4
Logistic regression between tract fiber-bundle cross-section (FC) and visual attention or visual communication score, with and without adjustment for known clinical confounders.

	Model corrected for PMA at MRI only		Model corrected for PMA at MRI and confounders*			Model corrected for PMA at MRI only		Model corrected for PMA at MRI and confounders*	
	Coef. (95% CI)	P Value	Coef. (95% CI)	P Value		Coef. (95% CI)	P Value	Coef. (95% CI)	P Value
Visual Attention[ξ]									
PTR(R)	3.528 (-3.989, 11.045)	0.358	−0.051 (-17.294, 17.192)	0.995	**PTR(L)**	4.645 (-3.078, 12.368)	0.238	3.864 (-12.180, 19.908)	0.637
ILF(R)	4.175 (-3.831, 12.181)	0.307	9.229 (-6.959, 25.416)	0.264	**ILF(L)**	4.510 (-3.357, 12.377)	0.261	6.869 (-8.639, 22.378)	0.385
IFOF(R)	4.006 (-3.957, 11.968)	0.324	6.086 (-12.834, 25.006)	0.528	**IFOF (L)**	5.204 (-2.825, 13.233)	0.204	9.045 (-7.569, 25.658)	0.286
SLF(R)	4.418 (-2.800, 11.635)	0.230	−0.388 (-13.249, 12.474)	0.953	**SLF(L)**	4.338 (-2.502, 11.177)	0.214	0.852 (-11.240, 12.943)	0.890
Splenium of CC	4.234 (-2.910, 11.379)	0.245	−2.573 (-16.726, 11.581)	0.722					
Visual Communication[ξ]									
PTR(R)	5.647 (0.258, 11.036)	*0.040*	6.389 (-3.404, 16.182)	0.201	**PTR(L)**	4.744 (-0.809, 10.298)	0.094	3.690 (-6.561, 13.941)	0.481
ILF(R)	6.207 (0.380, 12.034)	*0.037*	11.188 (-0.177, 22.552)	0.054	**ILF(L)**	4.916 (-0.696, 10.529)	0.086	5.891 (-4.693, 16.476)	0.275
IFOF(R)	5.253 (-0.465, 10.972)	0.072	6.468 (-6.036, 18.973)	0.311	**IFOF (L)**	4.201 (-1.507, 9.908)	0.149	1.677 (-11.432, 14.787)	0.802
SLF(R)	4.583 (-0.461, 9.626)	0.075	2.968 (-5.421, 11.356)	0.488	**SLF(L)**	3.600 (-1.125, 8.323)	0.135	0.257 (-8.349, 8.863)	0.953
Splenium of CC	3.837 (-1.092, 8.766)	0.127	−1.120 (-9.594, 7.355)	0.796					

*Adjusted for confounders including postmenstrual age at MRI scan, gestational age, severe retinopathy of the prematurity, and total brain volume.
Abbreviations: posterior thalamic radiations (PTR), inferior longitudinal fasciculus (ILF), inferior fronto-occipital fasciculus (IFOF), superior longitudinal fasciculus (SLF), corpus callosum (CC), postmenstrual age (PMA), right = R, left = L.
[ξ] PreViAs subdomain scores dichotomized based on monitoring cutoffs.

Table 5
Logistic regression between tract fiber density (FD) and visual attention or visual communication score, with and without adjustment for known clinical confounders.

	Model corrected for PMA at MRI only		Model corrected for PMA at MRI and confounders*			Model corrected for PMA at MRI only		Model corrected for PMA at MRI and confounders*	
	Coef. (95% CI)	P Value	Coef. (95% CI)	P Value		Coef. (95% CI)	P Value	Coef. (95% CI)	P Value
Visual Attention[ξ]									
PTR(R)	8.684 (-10.198, 27.566)	0.367	7.497 (-12.123, 27.116)	0.454	**PTR(L)**	18.744 (0.337, 37.151)	*0.046*	18.004 (-1.254, 37.261)	0.067
ILF(R)	10.691 (-8.031, 29.413)	0.263	8.979 (-10.730, 28.689)	0.372	**ILF(L)**	16.279 (-0.420, 32.979)	0.056	15.385 (-1.925, 32.696)	0.082
IFOF(R)	11.940 (-6.624, 30.504)	0.207	10.682 (-8.680, 30.043)	0.280	**IFOF (L)**	19.129 (1.224, 37.034)	*0.036*	18.389 (-0.071, 36.850)	0.051
SLF(R)	24.499 (1.050, 47.948)	*0.041*	26.806 (2.367, 51.245)	*0.032*	**SLF(L)**	20.921 (-3.689, 45.531)	0.096	21.231 (-4.011, 46.473)	0.099
Splenium of CC	9.401 (-5.003, 23.804)	0.201	7.831 (-8.176, 23.838)	0.338					
Visual Communication[ξ]									
PTR(R)	7.825 (-6.049, 21.700)	0.269	6.690 (-7.526, 20.905)	0.356	**PTR(L)**	13.038 (-0.435, 26.511)	0.058	11.648 (-2.256, 25.552)	0.101
ILF(R)	11.387 (-1.817, 24.590)	0.091	9.998 (-3.726, 23.722)	0.153	**ILF(L)**	11.982 (-0.313, 23.996)	0.051	10.791 (-1.597, 23.180)	0.088
IFOF(R)	9.671 (-3.840, 23.183)	0.161	8.292 (-5.743, 22.327)	0.247	**IFOF (L)**	14.169 (1.118, 27.219)	*0.033*	12.959 (-0.498, 26.415)	0.059
SLF(R)	15.343 (-0.674, 31.360)	0.060	16.432 (-0.004, 32.867)	0.050	**SLF(L)**	11.734 (-4.715, 28.183)	0.162	11.652 (-5.102, 28.406)	0.173
Splenium of CC	6.411 (-3.348, 16.170)	0.198	4.591 (-6.079, 15.261)	0.399					

*Adjusted for confounders including postmenstrual age at MRI scan, gestational age, and severe retinopathy of the prematurity.
Abbreviations: posterior thalamic radiations (PTR), inferior longitudinal fasciculus (ILF), inferior fronto-occipital fasciculus (IFOF), superior longitudinal fasciculus (SLF), corpus callosum (CC), postmenstrual age (PMA), right = R, left = L.
[ξ] PreViAs subdomain scores dichotomized based on monitoring cutoffs.

interrelated (i.e., changes in one metric can manifest over time as changes in the other), it is essential to consider FDC, the product of FD and FC, when evaluating the ability of white matter tracts to relay information (Dhollander et al., 2021). In our study, we observed positive associations between all three metrics at TEA and visual function measured by PreViAs scores, allowing us to assert that diminished microscopic (within-voxel) FD and macroscopic FC of several white matter tracts antecede early visual-behavioral difficulties in VPT infants. Preterm infants have previously shown reduced FD, FC, and FDC in brain regions such as the corpus callosum, corticospinal tract, optic

Table 6
White matter tract fiber density (FD), fiber cross-section (FC), and fiber density and cross-section (FDC) of very preterm infants with and without ROP diagnosis.

	No ROP Diagnosis (N = 132) Mean (SD)	**ROP Diagnosis (N = 59)** Mean (SD)	P value
Inferior Longitudinal Fasciculus (ILF)			
FD (R)	0.364 (0.427)	0.354 (0.042)	0.140
FD (L)	0.355 (0.045)	0.345 (0.046)	0.141
FC (R)	1.100 (0.092)	1.054 (0.100)	*0.002*
FC (L)	1.131 (0.095)	1.092 (0.105)	*0.014*
FDC (R)	0.396 (0.065)	0.370 (0.066)	*0.014*
FDC (L)	0.396 (0.069)	0.373 (0.072)	*0.035*
Inferior Fronto-Occipital Fasciculus (IFOF)			
FD (R)	0.354 (0.043)	0.346 (0.043)	0.246
FD (L)	0.355 (0.044)	0.343 (0.043)	0.082
FC (R)	1.099 (0.083)	1.046 (0.093)	*<0.001*
FC (L)	1.115 (0.084)	1.067 (0.097)	*<0.001*
FDC (R)	0.385 (0.063)	0.359 (0.065)	*0.011*
FDC (L)	0.391 (0.065)	0.363 (0.067)	*0.007*
Superior Longitudinal Fasciculus (SLF)			
FD (R)	0.273 (0.036)	0.277 (0.037)	0.489
FD (L)	0.270 (0.038)	0.270 (0.036)	0.979
FC (R)	1.168 (0.111)	1.104 (0.126)	*<0.001*
FC (L)	1.174 (0.118)	1.103 (0.128)	*<0.001*
FDC (R)	0.319 (0.062)	0.307 (0.068)	0.233
FDC (L)	0.318 (0.066)	0.299 (0.064)	0.073
Posterior Thalamic Radiations (PTR)			
FD (R)	0.349 (0.039)	0.345 (0.041)	0.500
FD (L)	0.352 (0.038)	0.341 (0.042)	0.073
FC (R)	1.109 (0.091)	1.062 (0.109)	*0.002*
FC (L)	1.127 (0.096)	1.090 (0.109)	*0.021*
FDC (R)	0.381 (0.062)	0.362 (0.068)	0.056
FDC (L)	0.390 (0.064)	0.367 (0.070)	*0.025*
Splenium of the Corpus Callosum (CC)			
FD	0.380 (0.050)	0.358 (0.052)	*0.005*
FC	1.122 (0.100)	1.053 (0.112)	*<0.001*
FDC	0.416 (0.078)	0.363 (0.078)	*<0.001*

*Abbreviations: right = R, left = L.

radiations, and cingulum (Pannek et al., 2018). FD, FC, and FDC have also illustrated the slower, long-term development of white matter tracts in preterm-born children at ages 7 and 13 years (Kelly et al., 2020). Our group previously found robust associations between FD, FC, and FDC of sensorimotor white matter tracts and early diagnosis of cerebral palsy in VPT infants (Chandwani et al., 2021). While the prior work was limited to the study of sensorimotor tracts, we recognized the importance of examining other white matter tracts that may be abnormal in VPT infants, as cerebral palsy often presents with cognitive and visual dysfunction. The current study extends our initial work by using fixel-based analysis to investigate abnormal visual development in comorbid disorders such as CVI.

In the preterm neonate, CVI is thought to result from encephalopathy of prematurity (e.g., following intraventricular hemorrhage or periventricular leukomalacia) that disrupts the visual pathways via the optic radiations or thalamocortical fibers (Madan et al., 2005; Philip and Dutton, 2014). While prior DTI-based studies have investigated the microstructure of the optic radiations in prematurity, none have demonstrated the pathological changes occurring at both the micro and macrostructural level in early visual development. Moreover, we examined the morphology of the PTR, ILF, IFOF, SLF, and splenium of the CC and found evidence that multiple white matter tracts of the visual pathways are involved in higher-order visual dysfunction. The optic radiations (often referred to as the PTR) are the primary afferent fiber bundles that transmit information from the lateral geniculate nucleus to the primary visual cortex. Two studies (Bassi et al., 2008; Groppo et al., 2014) found that FA of the optic radiations in 53 and a subset of 37 preterm infants at 30- and 42-weeks PMA, respectively, were significantly positively correlated with early visual assessment scores (Ricci et al., 2008). In another study of 36 preterm infants born between 29 and 41 weeks gestational age, Berman et al. (2009) found that FA of the optic radiations correlated significantly with visual fixation tracking scores. Our results support these findings, with FDC of the left PTR at TEA associated with visual attention of VPT infants, before and after confounder adjustment. Additional univariate analyses also showed that FD the left PTR was associated with visual attention, while FDC of the left PTR and FC of the right PTR were associated with visual communication. Microstructural alterations in the optic radiations were also observed in VPT infants at older ages, with a study by Thompson et al. (2013) finding higher MD/RD and lower FA associated with poor visual acuity.

The ILF connects the occipital lobe to the anterior temporal lobe and processes visual cues, playing a role in object recognition, reading, and other visually-guided behaviors (Herbet et al., 2018). The IFOF, functionally similar to the ILF, acts as a second fiber pathway between the occipital and frontal lobes (Ashtari, 2012). To our knowledge, no studies have explored the role of the ILF or IFOF in the early visual development of preterm infants. Vollmer et al. (2017) reported significantly lower FA in the bilateral ILF and IFOF in preterm-born children at ages 12–18 years, compared to term-born controls. The ILF has also been found to be compromised in older children with visual-perceptual impairment and diminished object recognition (Ortibus et al., 2011). In our cohort, the associations between ILF/IFOF micro and macrostructure by TEA and visual outcomes uniquely suggest the developmental importance of both tracts in early visual development.

The SLF, consisting of up to five subdivisions, connects the frontal cortices to the occipital, parietal, and temporal lobes (Kamali et al., 2014). This association tract transmits a variety of signals concerning motor function, visual perception, auditory-spatial information, and language articulation. While studies have explored the SLF in motor and language development in preterm populations, none have focused on its role in visual development (Bassi et al., 2008; Liu et al., 2010). Our results indicate that injury/immaturity to the SLF in VPT infants may impact their higher-order visual abilities, especially visual attention. Lastly, while the CC is known to transfer visual information across hemispheres (Gazzaniga and Freedman, 1973), we found no associations between fixel-based metrics of the splenium of the CC and visual outcomes in our cohort. However, the microstructure of the CC is known to be altered in motor impairments such as cerebral palsy, and aspects of motor coordination rely on visual processing (Rose et al., 2009; Thompson et al., 2011; Merhar et al., 2016; Parikh et al., 2019).

To evaluate the specificity of our findings in the nine tracts of interest, we also assessed the morphology of the bilateral uncinate fasciculus. In unadjusted analyses, we found that FDC of the left uncinate was associated with visual attention, and FDC of the bilateral uncinate was associated with visual communication. After adjusting for confounders, only the left uncinate remained significantly associated with visual communication ($p = 0.047$). The uncinate, a tract that connects the orbitofrontal cortex to the anterior temporal lobe, is implicated in object recognition and verbal fluency but has not been found to be affected in children with visual impairment. Our findings of the uncinate are unique but expected, as CVI is known to be a comorbid disorder of conditions like cerebral palsy, in which higher cognitive functions are found to be affected in up to 50% of children and can contribute to difficulties in communication, processing emotion, and learning (Novak et al., 2012).

Broadly, visual processing can be divided into two cortical pathways: a ventral stream, which projects from the parvocellular LGN through ventral regions of the visual cortex to the temporal lobe, and a dorsal

stream, which projects from the magnocellular LGN through dorsal areas of the visual cortex and area V5 to the parietal lobe. The ventral stream is responsible for the perception of form and color of objects, while the dorsal stream functions in motion perception, visuo-spatial awareness, and object localization (Goodale & Milner, 1992). Studies have shown a higher prevalence of motion integration deficits in preterm infants when compared to term-born infants, with form perception usually spared (Taylor et al., 2009; Leung et al., 2018). Thus, the dorsal stream is believed to be more vulnerable to the effects of prematurity on brain development. Of the white matter tracts we examined, the ILF and IFOF comprise functions of the ventral stream, while the SLF comprises functions of the dorsal stream (Schmahmann et al., 2008; Ortibus et al., 2011; Dick and Tremblay, 2012; Kim et al., 2020). Along with alterations found in the optic radiations, we observed diminished FD, FC, and FDC of tracts across the dorsal and ventral streams, suggesting that both pathways may be impacted. Deficits in dorsal and ventral visual stream processing have also been observed in preterm children with PVL and cerebral palsy, further indicating a widespread atypical processing in higher-order visual impairments (Cioni et al., 1997; Fazzi et al., 2004, 2007).

ROP is a disease characterized by abnormal growth of vasculature due to altered oxygen concentrations and blood flow in preterm birth. Children with ROP are more likely to have visual deficits such as reduced vision, strabismus, amblyopia, and refractive errors. While prior studies have found associations between ROP and alterations in the microstructure of the optic radiations, it is unclear whether the condition affects visuomotor development and other higher-order visual-behavioral functions in preterm infants (Leung et al., 2018). Our sub-analysis showed significant differences in FC and FDC across VPT infants with and without ROP diagnosis, suggesting that VPT infants with ROP may have concurrent aberrant visual pathway microstructure. Supporting studies have also found associations between ROP and cortical abnormalities in this population (Kline et al., 2019).

Our study has several limitations. For the early visual-behavioral assessment, we used the PreViAs questionnaire. While PreViAs is objectively scored and relatively easy to complete, it is not an established screening tool or ophthalmologic examination. As with other inventories assessing visual skills, the validity of parents' evaluations of their child's behavior is often scrutinized due to its inherent subjectivity (Garcia-Ormaechea et al., 2014; Pueyo et al., 2014). PreViAs has been validated against clinically diagnosed visual-behavioral impairments up to 2 years of age. Nevertheless, the results of this study will need to be validated at a later age for infants in our VPT cohort, with the use of another visual-behavioral assessment. Another potential limitation is the lack of correction for multiple comparisons. While false discovery rate correction can reduce the likelihood of making a type I error (i.e., false positives), it also increases the probability of a type II error (i.e., false negatives) occurring (Rothman, 1990). Because this study is the first to assess several visual pathway white matter tracts with the recently developed fixel-based analysis methodology, we felt it was more appropriate to not correct our results for multiple comparisons so we could provide greater insights into the pathophysiology of visual-behavioral difficulties in VPT infants and underscore the need for further investigation with preplanned hypotheses (Althouse, 2016). The strengths of our study include the large multi-center cohort of 191 VPT infants, novel use of advanced dMRI techniques such as CSD and fixel-based analysis, and systematic, highly reliable tractography methods. We also adjusted our analyses for known confounders that influence visual assessment, such as GA, ROP, and PMA at MRI scan.

5. Conclusion

In conclusion, we have shown that the micro and macrostructure of several white matter tracts is associated with visual-behavioral assessment scores in VPT infants at TEA. Infants born VPT can exhibit widespread reduced axonal density and tract cross-section in the major visual pathways, which may result in the development of more complex visual-behavioral problems later in life. While the present study only establishes the association between fixel-based metrics and early visual-behavioral scores, these metrics could also be valuable for predicting long-term visual outcomes. Functional connectivity and brain morphometric biomarkers that we and others have reported (Merhar et al., 2016; Weinstein et al., 2016; Kline et al., 2020a) should be explored in conjunction with fixel-based metrics to enable more robust prediction.

6. Funding information

This research was supported by grants R01-NS094200-05 and R01-NS096037-03 from the National Institute of Neurological Disorders and Stroke (NINDS), R01-EB029944-01 from National Institute of Biomedical Imaging and Bioengineering (NIBIB), and R21-HD094085 from the Eunice Shriver Kennedy National Institute of Child Health and Human Development (NICHD). The funders had no role in the study design, analysis, or presentation of findings.

CRediT authorship contribution statement

Rahul Chandwani: Methodology, Validation, Investigation, Writing – review & editing, Software, Formal analysis, Writing – original draft, Visualization, Data curation, Resources. **Karen Harpster:** Data curation, Investigation, Writing – review & editing. **Julia E. Kline:** Methodology, Validation, Investigation, Writing – review & editing, Software, Formal analysis, Writing – original draft, Visualization, Data curation, Resources. **Ved Mehta:** Data curation, Investigation, Writing – review & editing. **Hui Wang:** Data curation, Investigation, Writing – review & editing. **Stephanie L. Merhar:** Data curation, Investigation, Writing – review & editing. **Terry L. Schwartz:** Investigation, Writing – review & editing. **Nehal A. Parikh:** Conceptualization, Methodology, Investigation, Writing – review & editing, Funding acquisition, Formal analysis, Writing – original draft, Data curation, Supervision, Project administration, Resources.

Declaration of Competing Interest

The authors declare that they have no known competing financial interests or personal relationships that could have appeared to influence the work reported in this paper.

Acknowledgements

We sincerely thank the parents of infants that participated in our study and the Cincinnati Infant Neurodevelopment Early Prediction Study (CINEPS) Investigators: Principal Investigator: Nehal A. Parikh, DO, MS. Collaborators (in alphabetical order): Mekibib Altaye, PhD, Anita Arnsperger, RRT, Traci Beiersdorfer, RN BSN, Kaley Bridgewater, RT(MR) CNMT, Tanya Cahill, MD, Kim Cecil, PhD, Kent Dietrich, RT, Christen Distler, BSN RNC-NIC, Juanita Dudley, RN BSN, Brianne Georg, BS, Cathy Grisby, RN BSN CCRC, Lacey Haas, RT(MR) CNMT, Karen Harpster, PhD, OT/RL, Lili He, PhD, Scott K. Holland, PhD, V.S. Priyanka Illapani, MS, Kristin Kirker, CRC, Julia E. Kline, PhD, Beth M. Kline-Fath, MD, Hailong Li, PhD, Matt Lanier, RT(MR) RT(R), Stephanie L. Merhar, MD MS, Greg Muthig, BS, David Russell, JD, Kari Tepe, BSN RNC-NIC, Leanne Tamm, PhD, Julia Thompson, RN BSN, Jean A. Tkach, PhD, Hui Wang, PhD, Jinghua Wang, PhD, Brynne Williams, RT(MR) CNMT, Kelsey Wineland, RT(MR) CNMT, Sandra Wuertz, RN BSN CCRP, Donna Wuest, AS, Weihong Yuan, PhD.

Appendix A. Supplementary data

Supplementary data to this article can be found online at https://doi.org/10.1016/j.nicl.2022.102987.

References

Alexander, A.L., Hasan, K.M., Lazar, M., Tsuruda, J.S., Parker, D.L., 2001. Analysis of partial volume effects in diffusion-tensor MRI. Magn. Reson. Med. 45 (5), 770–780. https://doi.org/10.1002/mrm.1105.

Althouse, A.D., 2016. Adjust for Multiple Comparisons? It's Not That Simple. Ann. Thorac. Surg. 101 (5), 1644–1645. https://doi.org/10.1016/j.athoracsur.2015.11.024.

Ashtari, M., 2012. Anatomy and functional role of the inferior longitudinal fasciculus: a search that has just begun. Dev. Med. Child Neurol. 54, 6–7. https://doi.org/10.1111/j.1469-8749.2011.04122.x.

Auriat, A.M., Borich, M.R., Snow, N.J., Wadden, K.P., Boyd, L.A., 2015. Comparing a diffusion tensor and non-tensor approach to white matter fiber tractography in chronic stroke. NeuroImage: Clinical 7, 771–781. https://doi.org/10.1016/j.nicl.2015.03.007.

Bassi, L., Ricci, D., Volzone, A., Allsop, J.M., Srinivasan, L., Pai, A., Ribes, C., Ramenghi, L.A., Mercuri, E., Mosca, F., Edwards, A.D., Cowan, F.M., Rutherford, M. A., Counsell, S.J., 2008. Probabilistic diffusion tractography of the optic radiations and visual function in preterm infants at term equivalent age. Brain 131 (2), 573–582.

Berman, J.I., Glass, H.C., Miller, S.P., Mukherjee, P., Ferriero, D.M., Barkovich, A.J., Vigneron, D.B., Henry, R.G., 2009. Quantitative fiber tracking analysis of the optic radiation correlated with visual performance in premature newborns. AJNR Am. J. Neuroradiol. 30 (1), 120–124.

Chandwani, R., Kline, J.E., Harpster, K., Tkach, J., Parikh, N.A., 2021. Early micro- and macrostructure of sensorimotor tracts and development of cerebral palsy in high risk infants. Hum. Brain Mapp. 42 (14), 4708–4721.

Cioni, G., Bertuccelli, B., Boldrini, A., Canapicchi, R., Fazzi, B., Guzzetta, A., Mercuri, E., 2000. Correlation between visual function, neurodevelopmental outcome, and magnetic resonance imaging findings in infants with periventricular leukomalacia. Arch. Dis. Child. Fetal Neonatal Ed. 82 (2), F134–F140. https://doi.org/10.1136/fn.82.2.f134.

Cioni, G., Fazzi, B., Coluccini, M., Bartalena, L., Boldrini, A., van Hof-van Duin, J., 1997. Cerebral visual impairment in preterm infants with periventricular leukomalacia. Pediatr. Neurol. 17 (4), 331–338. https://doi.org/10.1016/s0887-8994(97)00152-5.

Committee on Practice and Ambulatory Medicine, Section on Ophthalmology. American Association of Certified Orthoptists, American Association for Pediatric Ophthalmology and Strabismus, & American Academy of Ophthalmology (2003). Eye examination in infants, children, and young adults by pediatricians. *Pediatrics, 111*(4 Pt 1), 902–907. https://doi.org/10.1542/peds.111.4.902.

Cotter, S.A., Cyert, L.A., Miller, J.M., Quinn, G.E., National Expert Panel to the National Center for Children's Vision and Eye Health, 2015. Vision screening for children 36 to <72 months: recommended practices. Optometry and Vision Science 92 (1), 6–16. https://doi.org/10.1097/OPX.0000000000000429.

Dhollander, T., Clemente, A., Singh, M., Boonstra, F., Civier, O., Duque, J., Caeyenberghs, K., 2021. Fixel-based Analysis of Diffusion MRI: Methods, Applications, Challenges and Opportunities. NeuroImage 241. https://doi.org/10.31219/osf.io/zu8fv.

Dick, S.A., Tremblay, P., 2012. Beyond the arcuate fasciculus: consensus and controversy in the connectional anatomy of language. Brain 135 (12), 3529–3550. https://doi.org/10.1093/brain/aws222.

Fazzi, E., Bova, S.M., Uggetti, C., Signorini, S.G., Bianchi, P.E., Maraucci, I., Zoppello, M., Lanzi, G., 2004. Visual-perceptual impairment in children with periventricular leukomalacia. Brain Dev. 26 (8), 506–512.

Fazzi, E., Signorini, S.G., Bova, S.M., La Piana, R., Ondei, P., Bertone, C., Misefari, W., Bianchi, P.E., 2007. Spectrum of visual disorders in children with cerebral visual impairment. J. Child Neurol. 22 (3), 294–301.

García-Ormaechea, I., González, I., Duplá, M., Andres, E., Pueyo, V., 2014. Validation of the Preverbal Visual Assessment (PreViAs) questionnaire. Early Human Dev. 90 (10), 635–638. https://doi.org/10.1016/j.earlhumdev.2014.08.002.

Gazzaniga, M.S., Freedman, H., 1973. Observations on visual processes after posterior callosal section. Neurology 23 (10), 1126–1130. https://doi.org/10.1212/WNL.23.10.1126.

Goodale, M.A., Milner, A.D., 1992. Separate visual pathways for perception and action. Trends Neurosci. 15, 20–25. https://doi.org/10.1016/0166-2236(92)90344-8.

Groppo, M., Ricci, D., Bassi, L., Merchant, N., Doria, V., Arichi, T., Allsop, J.M., Ramenghi, L., Fox, M.J., Cowan, F.M., Counsell, S.J., Edwards, A.D., 2014. Development of the optic radiations and visual function after premature birth. Cortex; a journal devoted to the study of the nervous system and behavior 56, 30–37.

Guzzetta, A., Cioni, G., Cowan, F., Mercuri, E., 2001. Visual disorders in children with brain lesions: 1. Maturation of visual function in infants with neonatal brain lesions: correlation with neuroimaging. EJPN 5 (3), 107–114. https://doi.org/10.1053/ejpn.2001.0480.

Harpster, K., Merhar, S., Illapani, V.S., Peyton, C., Kline-Fath, B., Parikh, N., 2021. Associations Between Early Structural Magnetic Resonance Imaging, Hammersmith Infant Neurological Examination, and General Movements Assessment in Infants Born Very Preterm. J. Pediatrics 232, 80–86.e2. https://doi.org/10.1016/j.jpeds.2020.12.056.

Herbet, G., Zemmoura, I., Duffau, H., 2018. Functional Anatomy of the Inferior Longitudinal Fasciculus: From Historical Reports to Current Hypotheses. Front. Neuroanat. 12, 77. https://doi.org/10.3389/fnana.2018.00077.

Jakobson, L.S., & Taylor, N.M. (2009). Differential vulnerability of cerebral visual functions in children born very prematurely. *Acta paediatrica (Oslo, Norway: 1992), 98*(2), 239-41. https://doi.org/10.1111/j.1651-2227.2008.01173.x.

Jeurissen, B., Leemans, A., Tournier, J.D., Jones, D.K., Sijbers, J., 2013. Investigating the prevalence of complex fiber configurations in white matter tissue with diffusion magnetic resonance imaging. Hum. Brain Mapp. 34 (11), 2747–2766. https://doi.org/10.1002/hbm.22099.

Jeurissen, B., Tournier, J.D., Dhollander, T., Connelly, A., Sijbers, J., 2014. Multi-tissue constrained spherical deconvolution for improved analysis of multi-shell diffusion MRI data. NeuroImage 103, 411–426. https://doi.org/10.1016/j.neuroimage.2014.07.061.

Kamali, A., Flanders, A.E., Brody, J., Hunter, J.V., Hasan, K.M., 2014. Tracing superior longitudinal fasciculus connectivity in the human brain using high resolution diffusion tensor tractography. Brain Struct. Funct. 219 (1), 269–281. https://doi.org/10.1007/s00429-012-0498-y.

Kaur, S., Powell, S., He, L., Pierson, C.R., Parikh, N.A., He, Y., 2014. Reliability and repeatability of quantitative tractography methods for mapping structural white matter connectivity in preterm and term infants at term-equivalent age. PLoS ONE 9 (1). https://doi.org/10.1371/journal.pone.0085807.

Kelly, C.E., Thompson, D.K., Genc, S., Chen, J., Yang, J.Y., Adamson, C., Anderson, P.J., 2020. Long-term development of white matter fibre density and morphology up to 13 years after preterm birth: A fixel-based analysis, 117068 NeuroImage 220. https://doi.org/10.1016/j.neuroimage.2020.117068.

Kidokoro, H., Neil, J.J., Inder, T.E., 2013. New MR imaging assessment tool to define brain abnormalities in very preterm infants at term. AJNR Am. J. Neuroradiol. 34 (11), 2208–2214. https://doi.org/10.3174/ajnr.A3521.

Kim, S.H., Jeon, H.E., Park, C.H., 2020. Relationship between Visual Perception and Microstructural Change of the Superior Longitudinal Fasciculus in Patients with Brain Injury in the Right Hemisphere: A Preliminary Diffusion Tensor Tractography Study. Diagnostics (Basel, Switzerland) 10 (9), 641. https://doi.org/10.3390/diagnostics10090641.

Kline, J.E., Illapani, V., He, L., Altaye, M., Parikh, N.A., 2019. Retinopathy of Prematurity and Bronchopulmonary Dysplasia are Independent Antecedents of Cortical Maturational Abnormalities in Very Preterm Infants. Sci. Rep. 9 (1), 19679. https://doi.org/10.1038/s41598-019-56298-x.

Kline, J.E., Illapani, V., He, L., Altaye, M., Logan, J.W., Parikh, N.A., 2020a. Early cortical maturation predicts neurodevelopment in very preterm infants. Arch. Dis. Child. Fetal Neonatal Ed. 105 (5), 460–465. https://doi.org/10.1136/archdischild-2019-317466.

Kline, J.E., Illapani, V.S., He, L., Parikh, N.A., 2020b. Automated brain morphometric biomarkers from MRI at term predict motor development in very preterm infants. NeuroImage: Clinical 28, 102475. https://doi.org/10.1016/j.nicl.2020.102475.

Lee, J., Kim, M.G., Park, H.Y., Nam, K.E., Park, J.H., 2021. Visual assessment of preterm and full-term infants under the age of 12 months using the Preverbal Visual Assessment questionnaire. Early Human Dev. 153, 105289 https://doi.org/10.1016/j.earlhumdev.2020.105289.

Leergaard, T.B., White, N.S., de Crespigny, A., Bolstad, I., D'Arceuil, H., Bjaalie, J.G., Dale, A.M., Valdes-Sosa, P.A., 2010. Quantitative histological validation of diffusion MRI fiber orientation distributions in the rat brain. PLoS ONE 5 (1). https://doi.org/10.1371/journal.pone.0008595.

Leung, M.P., Thompson, B., Black, J., Dai, S., Alsweiler, J.M., 2018. The effects of preterm birth on visual development. Clinical & experimental optometry 101 (1), 4–12. https://doi.org/10.1111/cxo.12578.

Liu, Y., Balériaux, D., Kavec, M., Metens, T., Absil, J., Denolin, V., Pardou, A., Avni, F., Van Bogaert, P., Aeby, A., 2010. Structural asymmetries in motor and language networks in a population of healthy preterm neonates at term equivalent age: a diffusion tensor imaging and probabilistic tractography study. NeuroImage 51 (2), 783–788.

Madan, A., Jan, J.E., Good, W.V., 2005. Visual development in preterm infants. Dev. Med. Child Neurol. 47 (4), 276–280. https://doi.org/10.1017/s0012162205000514.

Makropoulos, A., Robinson, E.C., Schuh, A., Wright, R., Fitzgibbon, S., Bozek, J., Counsell, S.J., Steinweg, J., Vecchiato, K., Passerat-Palmbach, J., Lenz, G., Mortari, F., Tenev, T., Duff, E.P., Bastiani, M., Cordero-Grande, L., Hughes, E., Tusor, N., Tournier, J.-D., Hutter, J., Price, A.N., Teixeira, R.P.A.G., Murgasova, M., Victor, S., Kelly, C., Rutherford, M.A., Smith, S.M., Edwards, A.D., Hajnal, J.V., Jenkinson, M., Rueckert, D., 2018. The developing human connectome project: A minimal processing pipeline for neonatal cortical surface reconstruction. NeuroImage 173, 88–112.

Malhotra, A., Sepehrizadeh, T., Dhollander, T., Wright, D., Castillo-Melendez, M., Sutherland, A.E., Pham, Y., Ditchfield, M., Polglase, G.R., de Veer, M., Jenkin, G., Pannek, K., Shishegar, R., Miller, S.L., 2019. Advanced MRI analysis to detect white matter brain injury in growth restricted newborn lambs. NeuroImage: Clinical 24. https://doi.org/10.1016/j.nicl.2019.101991.

Merhar, S.L., Gozdas, E., Tkach, J.A., Harpster, K.L., Schwartz, T.L., Yuan, W., Kline-Fath, B.M., Leach, J.L., Altaye, M., Holland, S.K., 2016. Functional and structural connectivity of the visual system in infants with perinatal brain injury. Pediatr. Res. 80 (1), 43–48.

Novak, I., Hines, M., Goldsmith, S., Barclay, R., 2012. Clinical prognostic messages from a systematic review on cerebral palsy. Pediatrics 130 (5), e1285–e1312. https://doi.org/10.1542/peds.2012-0924.

O'Connor, A.R., Wilson, C.M., Fielder, A.R., 2007. Ophthalmological problems associated with preterm birth. Eye (London, England) 21 (10), 1254–1260. https://doi.org/10.1038/sj.eye.6702838.

Ortibus, E.L., De Cock, P.P., Lagae, L.G., 2011. Visual perception in preterm children: what are we currently measuring? Pediatr. Neurol. 45 (1), 1–10. https://doi.org/10.1016/j.pediatrneurol.2011.02.008.

Pannek, K., Fripp, J., George, J.M., Fiori, S., Colditz, P.B., Boyd, R.N., Rose, S.E., 2018. Fixel-based analysis reveals alterations is brain microstructure and macrostructure of preterm-born infants at term equivalent age. NeuroImage. Clinical 18, 51–59. https://doi.org/10.1016/j.nicl.2018.01.003.

Parikh, N.A., 2016. Advanced neuroimaging and its role in predicting neurodevelopmental outcomes in very preterm infants. Semin. Perinatol. 40 (8), 530–541. https://doi.org/10.1053/j.semperi.2016.09.005.

Parikh, N.A., Hershey, A., Altaye, M., 2019. Early Detection of Cerebral Palsy Using Sensorimotor Tract Biomarkers in Very Preterm Infants. Pediatr. Neurol. 98, 53–60. https://doi.org/10.1016/j.pediatrneurol.2019.05.001.

Pascal, A., Govaert, P., Oostra, A., Naulaers, G., Ortibus, E., Van den Broeck, C., 2018. Neurodevelopmental outcome in very preterm and very-low-birthweight infants born over the past decade: a meta-analytic review. Dev. Med. Child Neurol. 60 (4), 342–355. https://doi.org/10.1111/dmcn.13675.

Blencowe, H., Lawn, J.E., Vazquez, T., Fielder, A., Gilbert, C., 2013. Preterm-associated visual impairment and estimates of retinopathy of prematurity at regional and global levels for 2010. Pediatric Res. 74 (Suppl 1), 35–49. https://doi.org/10.1038/pr.2013.205.

Philip, S.S., Dutton, G.N., 2014. Identifying and characterising cerebral visual impairment in children: a review. Clinical Exp. Optometry 97 (3), 196–208. https://doi.org/10.1111/cxo.12155.

Pueyo, V., García-Ormaechea, I., González, I., Ferrer, C., de la Mata, G., Duplá, M., Orós, P., Andres, E., 2014. Development of the Preverbal Visual Assessment (PreViAs) questionnaire. Early Human Dev. 90 (4), 165–168.

Raffelt, D., Tournier, J.-D., Rose, S., Ridgway, G.R., Henderson, R., Crozier, S., Salvado, O., Connelly, A., 2012. Apparent Fibre Density: A novel measure for the analysis of diffusion-weighted magnetic resonance images. NeuroImage 59 (4), 3976–3994.

Raffelt, D.A., Tournier, J.D., Smith, R.E., Vaughan, D.N., Jackson, G., Ridgway, G.R., Connelly, A., 2017. Investigating white matter fibre density and morphology using fixel-based analysis. NeuroImage 144, 58–73. https://doi.org/10.1016/j.neuroimage.2016.09.029.

Reijmer, Y.D., Leemans, A., Heringa, S.M., Wielaard, I., Jeurissen, B., Koek, H.L., Biessels, G.J., Zhan, W., 2012. Improved Sensitivity to Cerebral White Matter Abnormalities in Alzheimer's Disease with Spherical Deconvolution Based Tractography. PLoS ONE 7 (8). https://doi.org/10.1371/journal.pone.0044074.

Ricci, D., Anker, S., Cowan, F., Pane, M., Gallini, F., Luciano, R., Donvito, V., Baranello, G., Cesarini, L., Bianco, F., Rutherford, M., Romagnoli, C., Atkinson, J., Braddick, O., Guzzetta, F., Mercuri, E., 2006. Thalamic atrophy in infants with PVL and cerebral visual impairment. Early Human Dev. 82 (9), 591–595.

Ricci, D., Romeo, D.M.M., Haataja, L., van Haastert, I.C., Cesarini, L., Maunu, J., Pane, M., Gallini, F., Luciano, R., Romagnoli, C., de Vries, L.S., Cowan, F.M., Mercuri, E., 2008. Neurological examination of preterm infants at term equivalent age. Early Human Dev. 84 (11), 751–761.

Rojas-Vite, G., Coronado-Leija, R., Narvaez-Delgado, O., Ramírez-Manzanares, A., Marroquín, J.L., Noguez-Imm, R., Aranda, M.L., Scherrer, B., Larriva-Sahd, J., Concha, L., 2019. Histological validation of per-bundle water diffusion metrics within a region of fiber crossing following axonal degeneration. NeuroImage 201. https://doi.org/10.1016/j.neuroimage.2019.116013.

Rose, J., Butler, E.E., Lamont, L.E., Barnes, P.D., Atlas, S.W., Stevenson, D.K., 2009. Neonatal brain structure on MRI and diffusion tensor imaging, sex, and neurodevelopment in very-low-birthweight preterm children. Dev. Med. Child Neurol. 51, 526–535. https://doi.org/10.1111/j.1469-8749.2008.03231.x.

Rothman, K.J., 1990. No adjustments are needed for multiple comparisons. Epidemiology (Cambridge, Mass.) 1 (1), 43–46.

Schmahmann, J.D., Smith, E.E., Eichler, F.S., Filley, C.M., 2008. Cerebral white matter: neuroanatomy, clinical neurology, and neurobehavioral correlates. Ann. N. Y. Acad. Sci. 1142, 266–309. https://doi.org/10.1196/annals.1444.017.

Shah, D.K., Guinane, C., August, P., Austin, N.C., Woodward, L.J., Thompson, D.K., Warfield, S.K., Clemett, R., Inder, T.E., 2006. Reduced occipital regional volumes at term predict impaired visual function in early childhood in very low birth weight infants. Invest. Ophthalmol. Vis. Sci. 47 (8), 3366.

Taylor, N.M., Jakobson, L.S., Maurer, D., Lewis, T.L., 2009. Differential vulnerability of global motion, global form, and biological motion processing in full-term and preterm children. Neuropsychologia 47 (13), 2766–2778. https://doi.org/10.1016/j.neuropsychologia.2009.06.001.

Thompson, D.K., Inder, T.E., Faggian, N., Johnston, L., Warfield, S.K., Anderson, P.J., Doyle, L.W., Egan, G.F., 2011. Characterization of the corpus callosum in very preterm and full-term infants utilizing MRI. NeuroImage 55 (2), 479–490.

Thompson, D.K., Thai, D., Kelly, C.E., Leemans, A., Tournier, J.-D., Kean, M.J., Lee, K.J., Inder, T.E., Doyle, L.W., Anderson, P.J., Hunt, R.W., 2013. Alterations in the optic radiations of very preterm children-Perinatal predictors and relationships with visual outcomes. NeuroImage. Clinical 4, 145–153.

Tournier, J.D., Calamante, F., Connelly, A., 2007. Robust determination of the fibre orientation distribution in diffusion MRI: Non-negativity constrained super-resolved spherical deconvolution. NeuroImage 35 (4), 1459–1472. https://doi.org/10.1016/j.neuroimage.2007.02.016.

Tournier, J.D., Calamante, F., Connelly, A., 2013. Determination of the appropriate b value and number of gradient directions for high-angular-resolution diffusion-weighted imaging. NMR Biomed. 26 (12), 1775–1786. https://doi.org/10.1002/nbm.3017.

Tournier, J.D., Calamante, F., Gadian, D.G., Connelly, A., 2004. Direct estimation of the fiber orientation density function from diffusion-weighted MRI data using spherical deconvolution. NeuroImage 23 (3), 1176–1185. https://doi.org/10.1016/j.neuroimage.2004.07.037.

Tournier, J.D., Mori, S., Leemans, A., 2011. Diffusion tensor imaging and beyond. Magn. Reson. Med. 65 (6), 1532–1556. https://doi.org/10.1002/mrm.22924.

Tournier, J.-D., Smith, R., Raffelt, D., Tabbara, R., Dhollander, T., Pietsch, M., Christiaens, D., Jeurissen, B., Yeh, C.-H., Connelly, A., 2019. MRtrix3: A fast, flexible and open software framework for medical image processing and visualisation. NeuroImage 202. https://doi.org/10.1016/j.neuroimage.2019.116137.

Vollmer, B., Lundequist, A., Mårtensson, G., Nagy, Z., Lagercrantz, H., Smedler, A.-C., Forssberg, H., Baud, O., 2017. Correlation between white matter microstructure and executive functions suggests early developmental influence on long fibre tracts in preterm born adolescents. PLoS ONE 12 (6). https://doi.org/10.1371/journal.pone.0178893.

Wakana, S., Caprihan, A., Panzenboeck, M.M., Fallon, J.H., Perry, M., Gollub, R.L., Hua, K., Zhang, J., Jiang, H., Dubey, P., Blitz, A., van Zijl, P., Mori, S., 2007. Reproducibility of quantitative tractography methods applied to cerebral white matter. NeuroImage 36 (3), 630–644.

Walani, S.R., 2020. Global burden of preterm birth. Int. J. Gynaecol. Obstet. 150 (1), 31–33. https://doi.org/10.1002/ijgo.13195.

Weinstein, M., Ben-Sira, L., Moran, A., Berger, I., Marom, R., Geva, R., Gross-Tsur, V., Leitner, Y., Ben Bashat, D., 2016. The motor and visual networks in preterm infants: An fMRI and DTI study. Brain Res. 1642, 603–611.